Commun. Comput. Phys.
doi: 10.4208/cicp.180909.281209a

Vol. **8**, No. 2, pp. 427-444
August 2010

Implicit Unstructured-Mesh Method for Calculating Poiseuille Flows of Rarefied Gas

V. A. Titarev*

Fluid Mechanics and Computational Sciences Group, Aerospace Sciences Department, Cranfield University, Cranfield, MK43 0AL, UK.

Received 18 September 2009; Accepted (in revised version) 28 December 2009

Communicated by Chi-Wang Shu

Available online 12 March 2010

Abstract. An implicit high-order accurate method for solving model kinetic equations is proposed. The method is an extension of earlier work on the construction of an explicit TVD method for hybrid unstructured meshes in physical space and is illustrated on the Poiseuille flow of rarefied gas. Examples of calculations are provided for different Knudsen numbers and mesh resolutions, which illustrate the efficiency and high accuracy of the new scheme.

AMS subject classifications: 82D05, 76P05, 82B40, 82C40, 76M12, 65N08, 65B99

Key words: Poiseuille, kinetic, unstructured, mixed-element, micro, rarefied, implicit.

1 Introduction

The numerical solution of the Boltzmann kinetic equation with the exact or model collision integral is a major technique for studying rarefied gas flows. Usually, the numerical methods for this equation use structured meshes [10,11,28] and cannot be readily applied to flows in complex spatial configurations. Recently, high-order accurate finite-volume methods on unstructured meshes in physical space have been proposed. These include a Cartesian Cut Cell method for the Boltzmann equation with the exact collision integral [8] and an unstructured-mesh scheme [24] for the S-model kinetic equation [17, 18] in two spatial dimensions. In particular, the method [24] consists of two main components: an explicit high-order Total Variation Diminishing (TVD) scheme for discretising the advection operator on hybrid unstructured meshes and a conservative procedure for computing macroscopic gas parameters [23, 26]. It is thus applicable to gas flows in arbitrarily shaped two-dimensional spatial domains and across the whole range of

*Corresponding author. *Email addresses:* v.a.titarev@cranfield.ac.uk, titarev@mail.ru (V. A. Titarev)

 ©2010 Global-Science Press

Knudsen numbers from the free-molecular to continuum regimes. The method has been recently adopted to pressure-driven isothermal flows of rarefied gas in long micro channels (Poiseuille flow) [25], which represent an important class of rarefied gas dynamics problems [19,20]. Computational results were given for channels with circular, triangular and polygonal cross-sectional areas, thus showing the applicability of the unstructured-mesh approach in the context of rarefied gas flows.

All mentioned unstructured-mesh methods use explicit time discretisation methods. They are therefore simple to implement, but also computationally expensive as compared to implicit structured-mesh alternatives [11, 26, 28]. For transitional and nearly-continuum flows the stability condition of an explicit method results in a small time step, proportional to the spatial cell size in thin Knudsen layers. As a result, the computational cost of computing near-continuum steady-state solutions using explicit methods may be prohibitively high.

The goal of the present work is to develop an implicit version of the method [24, 25] for computing steady-state solutions of kinetic equations on two-dimensional unstructured meshes. For the sake of simplicity, the idea is explained for the linearised kinetic equation as applied to Poiseuille flows. On unstructured meshes, the use of the implicit time discretisation results in a large sparse system of linear equations for the values of the distribution function at the new time level. The direct solution of the system is expensive and requires the use of a large computer memory. To reduce the computational cost, an approximate factorisation based on [13, 14] is used. The resulting numerical method is almost as efficient per time step as the one-step explicit scheme with the same reconstruction procedure. However, it allows to use time step at least an order of magnitude larger as compared to the original explicit scheme. As a result, the overall computational cost of calculating the steady-state solutions is significantly reduced.

The paper is organised as follows. In Section 2 the flow problem and governing equations are formulated. In Section 3 the explicit method on mixed-element unstructured meshes [24,25] is briefly outlined. The implicit time discretisation scheme is described in detail in Section 4. In Section 5 numerical results are presented for the circular pipe flow and compared with those published in the literature. Conclusions are drawn in Section 6.

2 Problem formulation

Consider low-speed stationary flows of a monatomic rarefied gas from reservoir 1 to reservoir 2 through a channel with an arbitrary but constant cross-section A and finite length $2L$. Inside the reservoirs away from the channel the gas is at rest with pressures $p_1 < p_2$ and with equal temperatures $T_1 = T_2$. Let us introduce a Cartesian coordinate system (x,y,z), in which the Oz axes is directed along the channel. The centre of the coordinate system is located in the middle of the channel $z=0$. The complete accommodation of momentum and energy of molecules occurs at the channel walls, which are kept under the constant temperature $T_w = T_1 = T_2$. It is further assumed that the channel length

is much larger than the characteristic linear dimension D of its cross-sectional area.

A steady state of the rarefied gas is determined by the velocity distribution function $f(x,y,z,\xi_x,\xi_y,\xi_z)$, where ξ_x, ξ_y, ξ_z are the components of the molecular velocity vector $\boldsymbol{\xi}$. It is assumed that the distribution function satisfies the Boltzmann kinetic equation with the Krook model collision integral [3]:

$$\begin{aligned} &\xi_x\frac{\partial f}{\partial x}+\xi_y\frac{\partial f}{\partial y}+\xi_z\frac{\partial f}{\partial z}=\nu(f^o-f), \quad \nu=\frac{p}{\mu}, \\ &f^o=\frac{n}{(2\pi RT)^{3/2}}\exp(-c^2), \quad c_i=\frac{\xi_i-u_i}{\sqrt{2RT}}, \quad c^2=c_1^2+c_2^2+c_3^2, \quad i=1,2,3. \end{aligned} \tag{2.1}$$

Here n is gas density, u_i components of the velocity, T temperature, $p=nRT$ gas pressure, R the gas constant. The gas viscosity μ is related to the mean free path λ by

$$\mu=\frac{5}{16}mn\sqrt{2\pi RT}\lambda,$$

where m is the molecular mass. The boundary condition of diffuse reflection with the complete accommodation of momentum and energy of molecules on the channel surface ∂A reads as

$$\begin{aligned} &f(x,y,z,\xi_x,\xi_y,\xi_z)=f_w, \quad (\boldsymbol{\xi},\mathbf{n})>0, \\ &f_w=\frac{n_w(x,y,z)}{(2\pi RT_w)^{3/2}}\exp(-c_w^2), \quad c_w^2=\frac{\xi^2}{2RT_w}, \quad \xi^2=\xi_x^2+\xi_y+\xi_z^2, \end{aligned} \tag{2.2}$$

where $\mathbf{n}$ is the inward unit normal vector to the channel surface, n_w is the density of reflected molecules.

It is assumed that the average pressure (and thus density) gradient along the channel is small:

$$\frac{p_2-p_1}{L}\ll\frac{p_1}{D}.$$

so that the end effects can be neglected. The gas density near $z=0$ can then be expressed as a linear function of z

$$n_w(z)=n_0(1+k\cdot z), \quad kD=\frac{D}{n_0}\frac{dn_w(z)}{dz}\ll 1, \quad n_0=\frac{p_0}{T_w}, \quad p_0=\frac{1}{2}(p_1+p_2), \tag{2.3}$$

where k is the logarithmic derivative of density evaluated at $z=0$ and is assumed to be constant. The kinetic equation can be linearised around the Maxwellian distribution (2.2) with the density of reflected molecules n_w in the form (2.3):

$$f=f_w(1+h), \quad T\equiv T_w=\text{const}, \quad h=h(x,y,\boldsymbol{\xi}). \tag{2.4}$$

The equation for the function h is obtained by first inserting (2.4) in the nonlinear kinetic equation (2.1) and then using the assumption $|h|\ll 1$:

$$\xi_x\frac{\partial h}{\partial x}+\xi_y\frac{\partial h}{\partial y}=-\xi_z\cdot k+\nu_0(h^+-h), \quad h^+=2\xi_z u, \quad \nu_0=\frac{p_0}{\mu_0}. \tag{2.5}$$

Here u is gas velocity along the channel (in the z coordinate direction). The resulting kinetic equation (2.5) describes the flow near the middle section of the channel $z=0$.

In the rest of the paper the non-dimensional formulation of the problem is used, in which the following quantities serve as scales of spatial coordinates (x,y), velocity u, density n, temperature T and viscosity μ:

$$D, \quad \sqrt{2RT_w}, \quad n_0, \quad T_w, \quad \frac{5}{16}mn_0\sqrt{2\pi RT_w}\lambda_w.$$

Here λ_w is the mean free path, corresponding to n_0, T_w. Below, the non-dimensional variables are denoted by the same letters as the dimensional ones.

In the non-dimensional form the kinetic equation (2.5) for the function h takes the form

$$\xi_x\frac{\partial h}{\partial x}+\xi_y\frac{\partial h}{\partial y}=-\xi_z\cdot k+\nu_0(h^+-h), \quad h^+=2\xi_z u, \quad \nu_0=\frac{8}{5\sqrt{\pi}}\frac{1}{\mathrm{Kn}}. \tag{2.6}$$

Here $\mathrm{Kn}=\lambda_w/D$ is the Knudsen number. In what follows the value $k\equiv 1$ is used without loss of generality. The dimension of the problem can be reduced by passing from h to its integral with respect to ξ_z according to the formula

$$\phi=\int_{-\infty}^{+\infty}\xi_z g_0(\xi_z)h d\xi_z, \quad g_0(\xi_z)=\pi^{-1/2}e^{-\xi_z^2}.$$

The kinetic equation for the new function ϕ is obtained from (2.6) by multiplication by $\xi_z g_0(\xi_z)$ and integration with respect to ξ_z:

$$\xi_x\frac{\partial \phi}{\partial x}+\xi_y\frac{\partial \phi}{\partial y}=-\frac{1}{2}+\nu_0(\phi^+-\phi), \quad \phi^+=u. \tag{2.7}$$

The gas velocity is given as an integral of ϕ

$$u=\int\frac{1}{\pi}\phi\, e^{-\xi_x^2-\xi_y^2}d\xi_x d\xi_y. \tag{2.8}$$

The boundary condition (2.2) in terms of the function ϕ takes the form

$$\phi=0 \quad \text{for } (\boldsymbol{\xi},\boldsymbol{n})>0. \tag{2.9}$$

If the cross-sectional area of the channel has lines of symmetry, then it is possible to calculate the solution only in a part of the cross section, using reflective boundary condition on these symmetry lines [24]. This leads to a reduction of the computational cost.

One of the key integral parameters of the flow is the normalised mass flow rate through the channel, which in the non-dimensional variables is given by

$$Q=-\frac{2}{|A|}\int_A u dxdy=-\frac{2}{|A|}\int_A\int\frac{1}{\pi}\phi e^{-\xi_x^2-\xi_y^2}\, d\xi_x d\xi_y dxdy. \tag{2.10}$$

It is worth noting that in the free-molecular flow regime $\mathrm{Kn}=\infty$ the kinetic equation becomes degenerate for $\xi_x=\xi_y=0$ and the function ϕ has a singularity. This makes it difficult to solve equation numerically for $\mathrm{Kn}\gg 1$.

3 The explicit numerical method

Here the second-order accurate version of the explicit method from [24, 25] is reviewed. The kinetic equation (2.7) is solved in the unsteady formulation

$$\frac{\partial \phi}{\partial t}+\xi_x\frac{\partial \phi}{\partial x}+\xi_y\frac{\partial \phi}{\partial y}=-\frac{1}{2}+\nu_0(\phi^+-\phi),\quad \phi^+=u. \tag{3.1}$$

The steady-state solution to the problem is found by marching in time to steady state. Let us introduce in the physical variables $\boldsymbol{x}=(x_1,x_2)=(x,y)$ a computational mesh consisting of triangular and quadrilateral elements (spatial cells) E_i. The total number of spatial cells is N_{tot}. Each cell is defined by vertices with coordinates $\boldsymbol{x}^{(l)}$, $l=1,2,\cdots,L(i)$. In the molecular velocity space the infinite domain of integration is replaced by a finite computational domain $|\xi_x|,|\xi_y|\le\xi_0$, which is then discretised by N_ξ cells in each direction. The velocity distribution function is then defined in cell centers of both physical (x_i,y_i) and molecular velocity $\boldsymbol{\xi}_\alpha$ meshes.

Let $\phi^n_{i\alpha}$ be the spatial average of the velocity distribution function in the cell E_i at time t^n for the molecular velocity $\boldsymbol{\xi}_\alpha$. The unsplit fully discrete finite-volume method is obtained by integrating the kinetic equation (3.1) over the spatial cell E_i as well as the time interval:

$$\phi^{n+1}_{i\alpha}=\phi^n_{i\alpha}+\Delta t_\alpha L^n_{i\alpha},\quad L^n_{i\alpha}=-\frac{1}{2}-\frac{1}{|E_i|}\sum_{l=1}^{L(i)}\Phi_{i\alpha l}+\nu_0(\phi^+-\phi)^n_{i\alpha}, \tag{3.2}$$

where Δt_α is the time step size dependent on both the cell size $|E_i|$ and the module of the molecular velocity vector $\boldsymbol{\xi}_\alpha$. Let $\boldsymbol{n}_l=(n_x,n_y)$ be the outward unit normal vector to the side l; $\xi_{nl}=(\boldsymbol{\xi},\boldsymbol{n}_l)$ is the projection of the molecular velocity vector $\boldsymbol{\xi}_\alpha$ to the outward normal vector $\boldsymbol{n}_l$ to the side l (the index α is omitted for simplicity). Then the numerical flux $\Phi_{i\alpha l}$ through the side l of the cell E_i is given by

$$\Phi_{i\alpha l}=\int_{\boldsymbol{x}^{(l)}}^{\boldsymbol{x}^{(l+1)}}\xi_{nl}\phi^n(t,\boldsymbol{x},\boldsymbol{\xi}_\alpha)dl. \tag{3.3}$$

The calculation of the numerical fluxes with high-order of accuracy requires the knowledge of the values of the distribution function at cell sides. For each spatial cell E_i these values are computed from the cell averages of ϕ by means of a spatial reconstruction procedure [2, 22, 24, 25]. For the second-order method, which is used in the present study, the reconstruction stencil consists of the cell E_i and its direct neighbours. It is convenient to introduce the local numbering of cells in the stencils using a monoindex m, $m=0,\cdots,M$. The cells of the stencils and the corresponding values of the function ϕ are then referred to as T_m and $\phi^n_{m\alpha}$, respectively. In this notation T_0 corresponds to the cell E_i and T_m, $1\le m\le M$ correspond to its neighbours. The value of M depends on the shape of cell

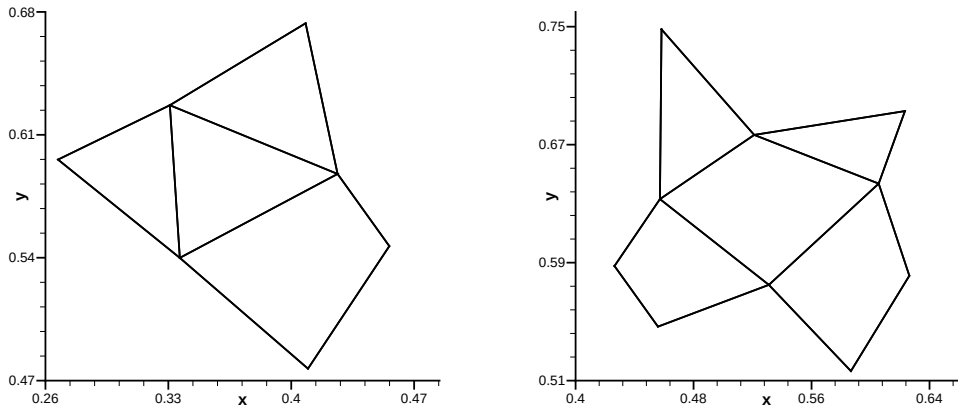

Figure 1: Possible stencils for the 2nd order reconstruction.

$E_i \equiv T_0$; for a quadrilateral cell $M=4$ whereas for a triangular cell $M=3$. Fig. 1 illustrates both cases.

In order to eliminate mesh scaling effects, which may affect the accuracy of the computations, the reconstruction is carried out in the local (reference) coordinate system $(\hat{x},\hat{y})$, which is obtained from the physical coordinate system (x,y) by means of a linear transformation [4,25]:

$$\boldsymbol{x}=\boldsymbol{x}^{(1)}+J_i\hat{\boldsymbol{x}}, \quad J_i=\begin{pmatrix} x^{(2)}-x^{(1)} & x^{(L(i))}-x^{(1)} \\ y^{(2)}-y^{(1)} & y^{(L(i))}-y^{(1)} \end{pmatrix}_i. \tag{3.4}$$

It should be stressed that the transformation matrix J_i is specific for the each cell E_i. The reconstruction stencil is then transformed into the reference coordinate system using the inverse transformation $\hat{\boldsymbol{x}}=\hat{\boldsymbol{x}}(\boldsymbol{x})$ and consists of transformed cells $\hat{T}_m$, $m=0,1,\cdots,M$. Note that the spatial averages of ϕ are not altered by the transformation.

For a given value of the molecular velocity vector $\boldsymbol{\xi}_\alpha$ the reconstruction polynomial $p_{i\alpha}(\hat{x},\hat{y})$ is considered to be an expansion over the basis functions $e_k(\hat{x},\hat{y})$ with the unknown coefficients a_1, a_2 called degrees of freedom:

$$\begin{aligned} &p_{i\alpha}(\hat{x},\hat{y})=\phi^n_{0\alpha}+a_1e_1(\hat{x},\hat{y})+a_2e_2(\hat{x},\hat{y}), \\ &e_1=\hat{x}-\frac{1}{|\hat{T}_0|}\int_{\hat{T}_0}\hat{x}d\hat{x}d\hat{y}, \quad e_2=\hat{y}-\frac{1}{|\hat{T}_0|}\int_{\hat{T}_0}\hat{y}d\hat{x}d\hat{y}. \end{aligned} \tag{3.5}$$

The unknown coefficients a_k of the polynomial (3.5) are calculated by requiring that for each cell $\hat{T}_m$ from the reconstruction stencil the mean value of $p_{i\alpha}$ is equal to the mean value of the solution:

$$\frac{1}{|\hat{T}_m|}\int_{\hat{T}_m}p_{i\alpha}(\hat{x},\hat{y})d\hat{x}d\hat{y}=\phi^n_{m\alpha}, \quad m=1,\cdots,M. \tag{3.6}$$

Conditions (3.6) can be re-written as the over-determined system for the unknown coefficients a_1, a_2:

$$f_{m1}a_1+f_{m2}a_2=\phi^n_{m\alpha}-\phi^n_{0\alpha},\quad f_{mk}=\frac{1}{|\hat{T}_m|}\int\limits_{\hat{T}_m}e_k(\hat{x},\hat{y})d\hat{x}d\hat{y},\quad m=1,\cdots,M, \tag{3.7}$$

which is solved by the least squares method. As a result, the values of a_k are expressed as a function of $\phi^n_{m\alpha}$ and local mesh geometry.

To suppress spurious oscillations in regions of rapid variations of the distribution function, a slope limiter ψ is used to modify the degrees of freedom a_1, a_2. Then the unlimited reconstruction polynomial $p_{i\alpha}$ defined in (3.5) is replaced by a new reconstruction polynomial

$$p^{\rm TVD}_{i\alpha}(\hat{x},\hat{y})=\phi^n_{0\alpha}+\psi_i[a_1e_1(\hat{x},\hat{y})+a_2e_2(\hat{x},\hat{y})]. \tag{3.8}$$

There are a number of slope limiters for the unstructured meshes, see [9] for review. Let $\phi_{\min}$, $\phi_{\max}$ be minimum and maximum values of the distribution function in the stencil. Also denote by p_l the average value of the unlimited polynomial (3.5) over the side l of the cell T'_0. The slope limiter [2] is given by

$$\psi_i=\min_l\psi_{il},\quad \psi_{il}=\begin{cases}\min(1,\Delta_1/\Delta_l), & p_l>\phi^n_{0\alpha},\\ \min(1,\Delta_2/\Delta_l), & p_l\le\phi^n_{0\alpha},\end{cases} \tag{3.9}$$

where

$$\Delta_1=\phi_{\max}-\phi^n_{0\alpha},\quad \Delta_2=\phi_{\min}-\phi^n_{0\alpha},\quad \Delta_l=p_l-\phi^n_{0\alpha}.$$

A smoother limiter is based on [27]:

$$\psi_i=\min_l\psi_{il},\quad \psi_{il}=\begin{cases}\dfrac{\Delta_1^2+2\Delta_l\Delta_1+\epsilon^2}{\Delta_1^2+\epsilon^2+2\Delta_l^2+\Delta_l\Delta_1}, & p_l>\phi^n_{0\alpha},\\ \dfrac{\Delta_2^2+2\Delta_l\Delta_2+\epsilon^2}{\Delta_2^2+\epsilon^2+2\Delta_l^2+\Delta_l\Delta_2}, & p_l\le\phi^n_{0\alpha},\end{cases} \tag{3.10}$$

where ϵ is a small parameter, which is the present work defined slightly differently than in [27] and is taken to be $\epsilon=\sqrt{E_i}$. Note, that the spatially first-order accurate reconstruction is reproduced if $\psi_i\equiv 0$.

Finally, for each cell E_i the averaged values $\phi^{(l)}_{i\alpha}$ of the reconstruction polynomial $p^{TVD}_{i\alpha}$ over each cell side l are computed according to the formula

$$\phi^{(l)}_{i\alpha}=\frac{1}{|\hat{\boldsymbol{x}}^{(l+1)}-\hat{\boldsymbol{x}}^{(l)}|}\int\limits_{\hat{\boldsymbol{x}}^{(l)}}^{\hat{\boldsymbol{x}}^{(l+1)}}p^{TVD}_{i\alpha}dl.$$

This completes the reconstruction step at time level t^n.

The calculation of the numerical fluxes $\Phi_{i\alpha l}$ is carried out as follows. If for the side l of the cell E_i the projection of the molecular velocity vector to the outward normal vector to the side l is non-negative $\xi_{nl} \geq 0$, then the numerical flux is given by

$$\Phi_{i\alpha l} = \xi_{nl} \phi_{i,\alpha}^{(l)} |\boldsymbol{x}^{(l)} - \boldsymbol{x}^{(l+1)}|.$$

If instead $\xi_{nl} < 0$, there are two cases to consider. If the side l is adjacent to the side l_1 of a fluid cell i_1, then the numerical flux is calculated as

$$\Phi_{i\alpha l} = \xi_{nl} \phi_{i_1\alpha}^{(l_1)} |\boldsymbol{x}^{(l)} - \boldsymbol{x}^{(l+1)}|. \tag{3.11}$$

If the side l is adjacent to the surface of the channel, the numerical flux is equal to zero, as is required by the boundary condition (2.9). For the spectacular reflection of the molecules the distribution function of reflected molecules was found by means of a parabolic interpolation in $\boldsymbol{\xi}$ and then inserted into the numerical flux formula.

The gas velocity u is found by integrating ϕ with respect to ξ_x, ξ_y in such a way that the resulting numerical method is conservative with respect to the model collision integral [23, 26]. For the linearised equation (3.1) the only conservation condition is the momentum conservation and the gas velocity is then given by [25]:

$$u_i^n = \frac{1}{\beta} \sum_\alpha e^{-\xi_\alpha^2} \phi_{i\alpha}^n \omega_\alpha, \quad \beta = \sum_\alpha e^{-\xi_\alpha^2} \omega_\alpha = \text{const}, \tag{3.12}$$

where ω_α are the weights of the composite integration rule. The choice of the quadrature rule depends on the flow regime. Typically, for $\delta \leq 10$ a non-uniform molecular velocity mesh clustered to $\xi_x = \xi_y = 0$ and second-order quadrature are used whereas for $\delta > 10$ the fourth-order accurate Simpson rule is applied on uniform meshes.

The normalised mass flow rate Q is calculated as

$$Q = -2 \frac{\sum\limits_i u_i |E_i|}{\sum\limits_i |E_i|}. \tag{3.13}$$

For the steady-state problems, considered in the present work, the time step size depends on the molecular velocity in order to speed up convergence to steady state:

$$\Delta t_\alpha = \min_i \left(K \frac{d_i}{|\xi_\alpha|}, 0.9\nu_0 \right), \quad K \leq \frac{1}{2}, \tag{3.14}$$

where K is the CFL number, d_i is a characteristic linear size of cell E_i. In general, for triangular elements, d_i is the diameter of the inscribed circle, whereas for quadrilateral elements d_i is taken to be the length of the largest side of element E_i.

It is worth noting that the resulting advection scheme (3.2) may be viewed as an extension of the second-order modification of the Godunov method [5] proposed in [7, 22].

The linear version of the method, based on the unlimited polynomial (3.5) is known to be unconditionally unstable. However, the presence of the limiter stabilizes the scheme under the condition (3.14). For more details see the original references [7, 22] as well as [9].

The convergence to steady state is verified by calculating the integral residual in the momentum conservation law:

$$R_{tot}=\sum_i |R_i|\cdot|E_i|\le 10^{-5},\quad R_i=\sum_\alpha L_{i\alpha}\frac{1}{\pi}\,e^{-\xi_\alpha^2}\omega_\alpha,$$

where the operator $L_{i\alpha}$ is defined in (3.2).

4 The implicit numerical method

The explicit scheme, described above, is quite simple to implement and provides highly-accurate results due to its applicability on general mixed-element meshes. However, for transitional and nearly-continuum flows the stability condition $K\le 1/2$ in (3.14) results in exceedingly small time steps, proportional to the spatial cell size in thin Knudsen layers. In practice, even smaller values $K=0.2,\cdots,0.3$ may be required for second and higher-order methods in order to achieve convergence to steady state. As a result, the computational cost of computing near-continuum steady-state solutions using the explicit method is quite high.

The implicit method described below can be viewed as an extension of the two-dimensional structured-mesh implicit methods of [6, 26, 28] to unstructured meshes. It circumvents the time step restrictions of the explicit scheme while maintaining its advantages, such as high-order spatial accuracy and simplicity of program implementation. Let ϕ_α^n be the value of the distribution function at the node $\boldsymbol{\xi}_\alpha$ of the molecular velocity mesh and time level t^n; the spatial variables x,y are kept continuum for the moment:

$$\phi_\alpha^n=\phi(t^n,x,y,\boldsymbol{\xi}_\alpha).$$

Define $\delta_{i\alpha}$ to be a time increment of the distribution function:

$$\delta_\alpha^n=\phi_\alpha^{n+1}-\phi_\alpha^n.$$

The explicit numerical method can be formally written as

$$\delta_\alpha^n=\Delta t_\alpha L_\alpha^n,\quad L_\alpha^n=-\frac{1}{2}-\left(\xi_x\frac{\partial\phi}{\partial x}+\xi_y\frac{\partial\phi}{\partial y}\right)_\alpha^n+\nu_0(\phi^+-\phi)_\alpha^n. \tag{4.1}$$

The implicit version of (4.1) is constructed by adding the advection and relaxation operators to the left-hand side:

$$\left(1+\Delta t_\alpha\nu_0+\Delta t_\alpha\xi_x\frac{\partial}{\partial x}+\Delta t_\alpha\xi_y\frac{\partial}{\partial y}\right)\delta_\alpha^n=\Delta t L_\alpha^n. \tag{4.2}$$

The resulting equation (4.2) forms the basis of the implicit finite-volume method, used below. In order to pass from the differential form (4.2) to the discrete scheme, the advection operator in the left-hand side of (4.2) is discretised with first-order upwind spatial differences on the given unstructured mesh in (x,y) variables whereas the right-hand side L_α^n is approximated in the same way as in the explicit method (3.2). Let $\sigma_l(i)$ be the cell index of the cell adjacent to the side l of cell E_i. Then the implicit finite-volume method based on (4.2) has the following form

$$(1+\Delta t_\alpha \nu_0)\delta_{i\alpha}^n + \frac{\Delta t_\alpha}{|E_i|}\sum_{l=1}^{L(i)} \xi_{nl} f(\delta_{i\alpha}^n, \delta_{\sigma_l(i),\alpha}^n) b_{il} = \Delta t_\alpha L_{i\alpha}^n, \quad \delta_{i\alpha}^n = \phi_{i\alpha}^{n+1} - \phi_{i\alpha}^n. \tag{4.3}$$

Here $b_{il} = |\boldsymbol{x}^{(l)} - \boldsymbol{x}^{(l+1)}|$ is the length of side l of the cell E_i. The function $f(\delta_{i\alpha}^n, \delta_{\sigma_l(i),\alpha}^n)$ plays a role analogous to a Riemann solver in Godunov-type methods and is defined as

$$f(\delta_{i\alpha}^n, \delta_{\sigma_l(i),\alpha}^n) = \frac{1}{2}(1+\mathrm{sign}(\xi_{nl}))\cdot\delta_{i\alpha}^n + \frac{1}{2}(1-\mathrm{sign}(\xi_{nl}))\cdot\delta_{\sigma_l(i),\alpha}^n.$$

If the side l of cell E_i belongs to a solid boundary and $\xi_{nl}<0$, then the corresponding time increment δ in the neighbouring cell is set to zero. Regrouping terms in (4.3) yields the following

$$\begin{aligned} &(1+\Delta t_\alpha \nu_0 + \Delta t_\alpha b_i)\delta_{i\alpha}^n + \Delta t_\alpha \sum_{l=1}^{L(i)} c_{i,\sigma_l(i)} \delta_{\sigma_l(i),\alpha}^n = \Delta t_\alpha L_{i\alpha}^n, \\ &b_i = \sum_{l=1}^{L(i)} \xi_{n,l}(1+\mathrm{sign}(\xi_{nl}))\frac{b_{il}}{2|E_i|}, \quad c_{i,\sigma_l(i)} = \xi_{n,l}(1-\mathrm{sign}(\xi_{nl}))\frac{b_{il}}{2|E_i|}. \end{aligned} \tag{4.4}$$

The expressions (4.4) can then be re-written in matrix form as

$$\boldsymbol{Q}\cdot\boldsymbol{\delta}_\alpha^n = \Delta t_\alpha \boldsymbol{L}_\alpha^n, \tag{4.5}$$

where the elements q_{ij} of the matrix $\boldsymbol{Q}$ are defined as:

$$q_{ii} = 1+\Delta t_\alpha \nu_0 + \Delta t_\alpha b_i, \quad q_{i,\sigma_l(i)} = \Delta t_\alpha c_{i,\sigma_l(i)}, \quad l = 1,\cdots,L(i).$$

The matrix $\boldsymbol{Q}$ is sparse and diagonally dominant. However, the direct solution of the linear system (4.5) is very expensive and may not justify the use of the implicit method. Instead, an approximate factorisation of $\boldsymbol{Q}$ is used in order to construct a computationally efficient time marching algorithm [13, 14]. The implicit scheme (4.4) is re-written as

$$\begin{aligned} &\delta_{i\alpha}^n + \sum_{l=1}^{L(i)} \Delta t_\alpha \tilde{c}_{i,\sigma_l(i)} \delta_{\sigma_l(i),\alpha}^n = \Delta t_\alpha d_{ii}^{-1} L_{i\alpha}^n, \\ &d_{ii} = 1+\Delta t_\alpha \nu_0 + \Delta t_\alpha b_i, \quad \tilde{c}_{i,\sigma_l(i)} = \frac{1}{d_{ii}} c_{i,\sigma_l(i)}, \end{aligned} \tag{4.6}$$

or in the matrix form

$$(\boldsymbol{I}+\Delta t_\alpha \tilde{\boldsymbol{C}})\cdot\delta_\alpha^n=\Delta t_\alpha \boldsymbol{D}^{-1}\cdot \boldsymbol{L}_\alpha^n, \tag{4.7}$$

where $\boldsymbol{D}$ is the diagonal matrix with elements d_{ii} defined in (4.6). The matrix $\tilde{\boldsymbol{C}}$ is then factorised into the product of lower triangular $\boldsymbol{L}$ and upper triangular $\boldsymbol{U}$ matrices according to the formula

$$l_{ij}=\begin{cases}\Delta t_\alpha \tilde{c}_{ij}, & j<i,\\ 0, & j>i,\end{cases} \qquad u_{ij}=\begin{cases}0, & j<i,\\ \Delta t_\alpha \tilde{c}_{ij}, & j>i,\end{cases} \qquad l_{ii}=u_{ii}=1.$$

Finally, the approximate factorisation of the left-hand side of (4.7) is given by

$$\boldsymbol{I}+\Delta t_\alpha \tilde{\boldsymbol{C}}=\boldsymbol{L}\cdot\boldsymbol{U}+\mathcal{O}(\Delta t_\alpha^2) \tag{4.8}$$

so that the implicit method takes its final form

$$\boldsymbol{L}\cdot\boldsymbol{U}\delta_\alpha^n=\Delta t_\alpha \boldsymbol{D}^{-1}\cdot\boldsymbol{L}_\alpha^n, \quad \phi_{i\alpha}^{n+1}=\phi_{i\alpha}^n+\delta_{i\alpha}^n. \tag{4.9}$$

The computational cost of solving (4.9) is linearly proportional to the total number of spatial cells N_{tot}. As a result, one time step of the implicit scheme (4.9) is only slightly more expensive than that of the explicit one (3.2), most of the computational cost of both methods being associated with the spatial reconstruction procedure. For the nonlinear model kinetic equations, e.g., [1, 16, 18], this difference will be even smaller due to the high computational cost of the calculation of the collision integral.

The time step is now selected according to the formula

$$\Delta t_\alpha=K\cdot\frac{\min\limits_i d_i}{|\xi_\alpha|}, \tag{4.10}$$

where K is again the user-defined CFL number.

5 Results

The performance of the method is illustrated as applied to the Poiseuille flow in the channel with a circular cross section (circular pipe). The main parameter to be calculated is the normalised mass flow rate Q, which depends on the Knudsen number and the shape of the cross-sectional area. In the existing literature the so-called rarefaction parameter δ is often used instead of the Knudsen number when presenting the results. In the present work this parameter coincides with the collision frequency ν_0:

$$\delta\equiv\nu_0=\frac{8}{5\sqrt{\pi}}\frac{1}{\mathrm{Kn}}=\frac{1.1078}{\mathrm{Kn}}, \quad \mathrm{Kn}=\frac{0.9027}{\delta}.$$

A review of existing results for the Poiseuille flow through the circular pipe can be found [19, 20]. The free-molecular value of the mass flow rate can be evaluated analytically and is equal to $Q=Q_\infty\approx 1.5045$. For finite values of δ the most accurate analysis

was carried out in [12] by using a highly specialised numerical algorithm, developed specifically for flow in the circular pipe. The algorithm is based on solving the integral equations and makes use of the polar coordinate system and very high-order quadrature formulas. Furthermore, for the transitional and near-continuum regimes $\delta \gg 1$ the kinetic solution was computed as a correction to the continuum (Navier-Stokes) solution, resulting in accurate results up to $\delta = 500$. It should also be noted that for conventional finite-difference methods applied to the kinetic equation in the polar coordinate system the results have only be presented up to $\delta = 50$ even though the lower dimension of the problem allowed the use of very fine computational meshes, see, e.g., [21].

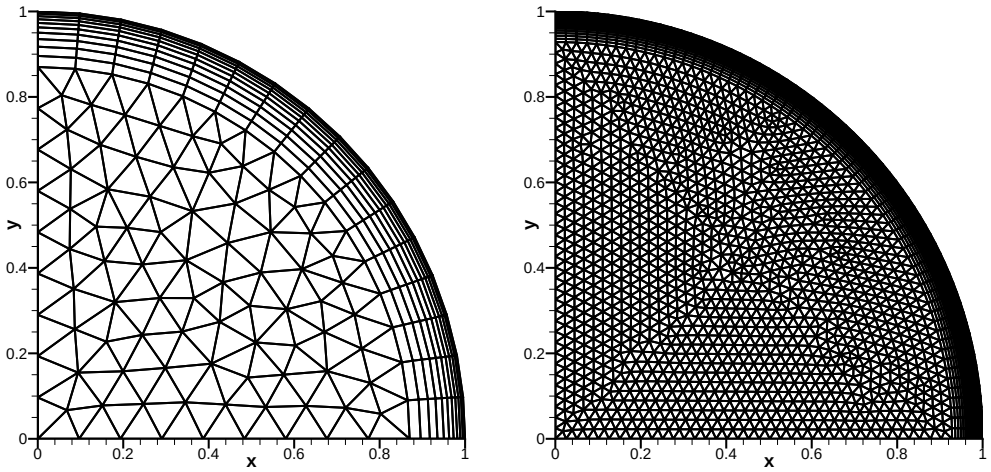

Figure 2: Computational domain and the spatial meshes with $N_{tot} = 330$ (left) and 3947 (right).

In the present work the mass flow rate for the Poiseuille flow in the circular channel is computed for $0 \leq \delta \leq 200$ using the general numerical algorithm (4.2), applicable to any cross-section form. In calculations the circular cross section was replaced by a 90 degrees sector and the reflective boundary condition was used on the radial sides of the computational domain. This allows the reduction of the computational cost of the simulations. Three spatial meshes were considered for a mesh convergence study, consisting of $N_{tot} = 330$, 1081 and 3947 cells, see Fig. 2. For $N_{tot} = 330$ the Knudsen layer near the surface is discretised with quadrilateral cells with length ≈ 0.005 in the direction normal to the surface, the boundaries of the spatial domain are divided into intervals of constant length 0.1 and then the inner part of the computational domain is meshed with triangles. Other meshes are obtained from the $N_{tot} = 330$ mesh using refining by a factor of two and four, respectively.

The integration in the molecular velocity space was carried out over the finite domain $-3.5 \leq \xi_x, \xi_y \leq 3.5$. For small and medium values of the rarefaction parameter $0 \leq \delta \leq 1$ (large Knudsen numbers) the distribution function varies very rapidly near $\xi_x = \xi_y = 0$ so that a relatively fine molecular velocity mesh with $N_\xi = 80$ cells in each direction had to

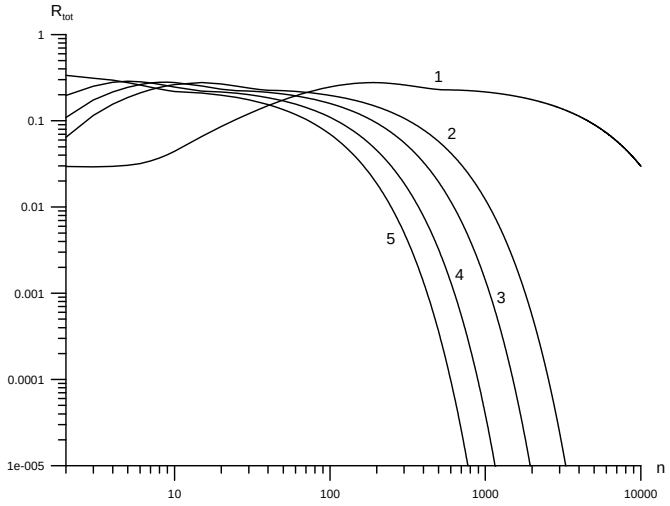

Figure 3: Convergence history for $N_{tot}=1081$ and $\delta=10$. First-order reconstruction is used. Curve 1 represents the explicit method with $K=0.3$ whereas 2-5 correspond to the values of CFL number $K=5$, 10, 25 and 100; n is the iteration number.

be used. The mesh was clustered towards the singularity point with the cell size near it equal to $\Delta\xi\approx 0.003$. For the transitional and near-continuum regimes $\delta>1$ of the flow the function ϕ varies slowly in the molecular velocity space so that a much coarser uniform mesh with constant cell size $\Delta\xi\approx 0.35$ was sufficient to obtain accurate results.

Figs. 3-5 illustrate the influence of the CFL number on the convergence history of the method; shown is the residual as a function of the iteration number n for the explicit method as well as the implicit one with $K=5$, 10, 25 and 100. All versions of the spatial reconstruction are used: 1st order as well as 2nd order with limiters (3.9) and (3.10). The results are provided for the middle mesh with $N_{tot}=1081$ and the value of the rarefaction parameter $\delta=10$; the converged solution for $\delta=1$ is used as the initial condition for time marching. It is seen that for the first-order accurate version of the method the implicit time marching provides at least an order of magnitude speed-up in convergence with larger values of the Courant number K resulting in fewer iterations required to reach the residual tolerance value $R_{tot}=10^{-5}$. For the second-order version of the method the convergence history depends significantly on the choice of the slope limiter. If (3.9) is used, the residual rapidly drops to $R_{tot}\approx 10^{-3}$, but then the convergence stalls. The use of the smoother limiter (3.10) considerably improves the convergence properties of the method with the residual dropping to 10^{-5} for $K=5$ and $K=10$. However, for larger values of the Courant number the residual drops to $\approx 10^{-4}$ only, which may be explained by the fact that the factorisation error in (4.8) becomes larger as K grows. Overall, $K=5,\cdots,10$ appears to be a good choice of the CFL number for the 2nd order method. For the rest of the paper all second-order results correspond to the choice of (3.10) for the slope limiter.

The results of the calculations for the mass flow rate for all values of δ using the

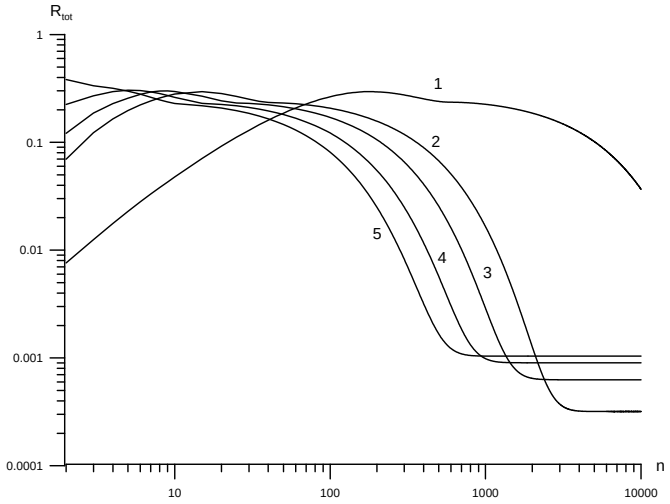

Figure 4: Convergence history for $N_{tot}=1081$ and $\delta=10$. 2nd order reconstruction with (3.9) limiter is used. Curve 1 represents the explicit method with $K=0.3$ whereas 2-5 correspond to the values of CFL number $K=5$, 10, 25 and 100; n is the iteration number.

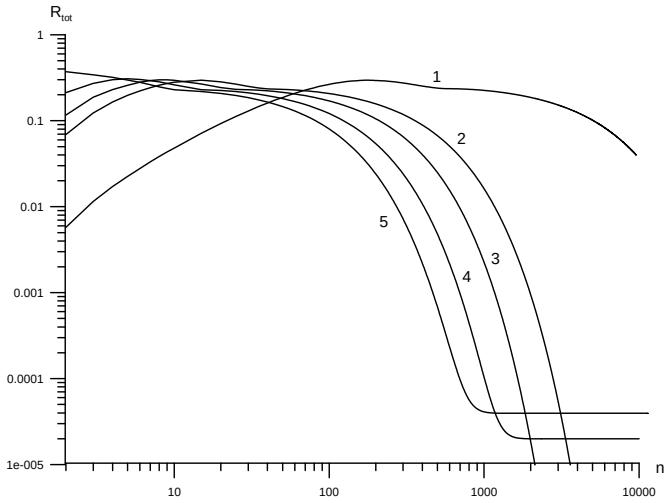

Figure 5: Convergence history for $N_{tot}=1081$ and $\delta=10$. 2nd order reconstruction with (3.10) limiter is used. Curve 1 represents the explicit method with $K=0.3$ whereas 2-5 correspond to the values of CFL number $K=5$, 10, 25 and 100; n is the iteration number.

implicit method with both 1st and 2nd order accurate spatial reconstructions are given in Tables 1 and 2. Also provided are the reference mass flow rate values from [12]. It is seen that the 1st order version of the method produces acceptable results for small and moderate values of the rarefaction parameter $0 \leq \delta \leq 1$, but starts to diverge from the reference solution as δ increases and the flow approaches transitional regime. This is explained by the fact that for $\delta \gg 1$ (or $\mathrm{Kn} \ll 1$) the numerical viscosity of the 1st order method prevails over the physical viscosity and the numerical solution is thus inaccurate.

Table 1: Normalised mass flow rate Q for the cylindrical pipe, 1st order method.

δ	$N_{tot}=330$	$N_{tot}=1081$	$N_{tot}=3947$	[12]
0.0	1.530318	1.517538	1.510286	1.5045
0.3	1.393437	1.385310	1.380652	1.3762
0.5	1.400897	1.394048	1.390139	1.3866
1	1.465376	1.461514	1.459472	1.4582
10	3.166507	3.313548	3.417102	3.5633
20	4.704936	5.152908	5.503968	6.0411
50.	7.762911	9.238882	10.679545	13.5269
100	10.631086	13.490859	15.710244	26.0214
200	13.585523	18.227347	21.734972	51.0254

Table 2: Normalised mass flow rate Q for the cylindrical pipe, 2nd order method.

δ	$N_{tot}=330$	$N_{tot}=1081$	$N_{tot}=3947$	[12]
0.0	1.501842	1.502524	1.502724	1.5045
0.3	1.374541	1.375689	1.376060	1.3762
0.5	1.384777	1.386098	1.386460	1.3866
1	1.455880	1.457605	1.458087	1.4582
10	3.533018	3.554309	3.560475	3.5633
20	5.9404	6.012289	6.032977	6.0411
50.	12.9646	13.367275	13.475604	13.5269
100	23.936042	25.410952	25.821233	26.0214
200	43.584960	48.673164	50.219904	51.0254

The 2nd order version of the method provides significantly more accurate results, which agree well with [12] in the whole range $0\leq\delta\leq200$. For small and moderate values of $\delta\leq1$ already the middle mesh with $N_{tot}=838$ provides sufficient accuracy. The largest difference in the flow rate occurs for $\delta=200$ and is below 2% for the finest mesh. It can also be concluded from Table 2 that the difference between results from two finest spatial meshes can serve as a safe upper estimate of the computational error, which can be used for other, more difficult geometries, for which no reference or exact solution is available.

For large values of δ the distribution function is smooth and thus the numerical error is defined mainly by the spatial resolution. In this case it is possible to increase the accuracy by using the Richardson extrapolation technique [15]. Denote by $Q^{(1)}$, $Q^{(2)}$, $Q^{(3)}$ the values of the mass flow rate calculated on three consecutive meshes with total number of cells $N_{tot}^{(1)}$, $N_{tot}^{(2)}$, $N_{tot}^{(3)}$. It is then assumed that for each mesh the exact value of the mass flow rate can be related to the computed value

$$Q^{exact}=Q^{(k)}+C\cdot h_k^p+o(h_k^p),\quad C=\text{const},\quad k=1,2,3, \tag{5.1}$$

where $h_k=1/\sqrt{N_{tot}^{(k)}}$ is the characteristic cell size. The spatial convergence rate p and the

Table 3: Richardson extrapolated values for the mass flow rate Q.

δ	20	50	100	200
Ref. [12]	6.0411	13.5269	26.0214	51.0254
Q^{ext}	6.0397	13.5077	25.9485	50.7638
Q for $N_{tot}=3947$	6.0330	13.4756	25.8212	50.2199
Estimate of p	2.17	2.28	2.23	2.08

constant C can be estimated from Eq. (5.1) and the extrapolated mass flow rate is then given by

$$Q^{ext}=Q^{(3)}+C\cdot h_3^p. \tag{5.2}$$

Provided that the spatial resolution is sufficiently fine, the expression (5.2) should give at least a third-order accurate approximation to the mass flow rate Q. Results of the application of Richardson extrapolation are shown in Table 3. It is seen that the numerical error in calculating Q is reduced significantly.

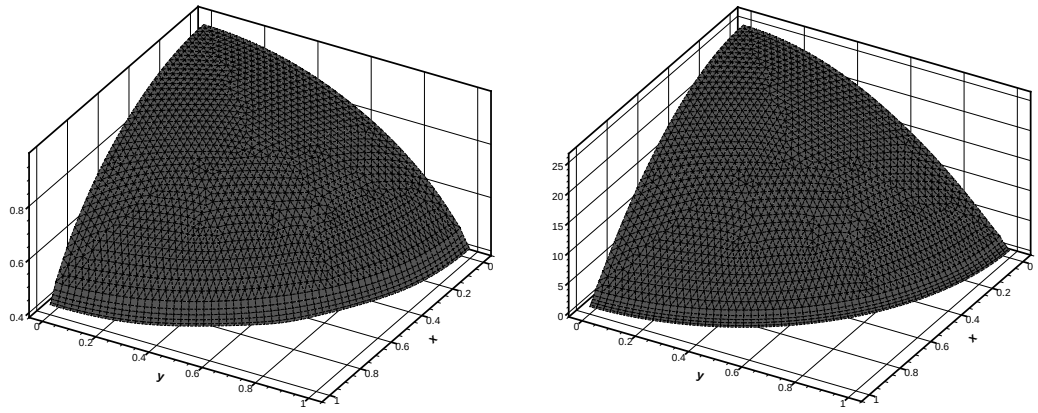

Figure 6: Velocity surfaces for $\delta=1$ (left) and $\delta=100$ (right).

Fig. 6 shows surface plots of the gas velocity u_z for two values of the rarefaction parameter: $\delta=1$ and $\delta=100$. It is seen that the numerical solution is radial without any numerical artefacts. The velocity field has a maximum at $x=y=0$ and drops towards the surface of the channel.

6 Conclusions

An implicit high-order accurate method for calculating the Poiseuille flow of a rarefied gas in channels with non-Cartesian cross-sectional areas has been developed. The use of the implicit time marching results in between one to two orders of magnitude speed

up in convergence to the steady-state solution. Numerical results for the circular pipe illustrate the efficiency as well as high accuracy of the new scheme in a broad range of flow regimes. The use of the Richardson extrapolation further increases the accuracy of the numerical results in the transitional and continuum regimes.

Acknowledgments

The author would like to thank Professor Evgeny Timofeev, McGill University, Canada, for very useful discussions regarding the construction of implicit methods on unstructured meshes as well as the two anonymous referees for their remarks that helped improve the quality of this work.

References

[1] P. Andries, K. Aoki, and B. Perthame. A consistent BGK-type model for gas mixtures. Journal of Statistical Physics, 106:993–1018, 2002.

[2] T.J. Barth and P.O. Frederickson. Higher order solution of the Euler equations on unstructured grids using quadratic reconstruction. In AIAA paper no. 90-0013, 28th Aerospace Sciences Meeting, 1990.

[3] P.L. Bhathnagar, E.P. Gross, and M. Krook. A model for collision processes in gases. I. Small amplitude processes in charged and neutral one-component systems. Phys. Rev., 94(511):1144–1161, 1954.

[4] M. Dumbser and M Käser. Arbitrary high order non-oscillatory finite volume schemes on unstructured meshes for linear hyperbolic systems. Journal of Computational Physics, 221(2):693–723, 2007.

[5] S.K. Godunov. A finite difference method for the computation of discontinuous solutions of the equations of fluid dynamics. Mat. Sbornik, 47:357–393, 1959.

[6] M.Ya. Ivanov and R.Z. Nigmatullin. Implicit scheme of S.K. Godunov with increased order of accuracy for Euler equaitons. USSR Comp. Math. Math. Phys., 27(11):1725–1735, 1987.

[7] V.P. Kolgan. Application of the minimum-derivative principle in the construction of finite-difference schemes for numerical analysis of discontinuous solutions in gas dynamics. Transactions of the Central Aerohydrodynamics Institute, 3(6):68–77, 1972. in Russian.

[8] V.I. Kolobov, R.R. Arslanbekov, V.V. Aristov, A.A. Frolova, and S.A. Zabelok. Unified solver for rarefied and continuum flows with adaptive mesh and algorithm refinement. J. Comp. Phys., 223:589–608, 2007.

[9] A.G. Kulikovskii, N.V. Pogorelov, and A.Yu. Semenov. Mathematical Aspects of Numerical Solution of Hyperbolic Systems. Chapman and Hall, 2002. Monographs and Surveys in Pure and Applied Mathematics, Vol. 118.

[10] I. N. Larina and V. A. Rykov. Investigation of the rarefied gas flow around a circular cylinder in stationary and oscillatory regimes. Fluid Dynamics, (1):152–160, 2006.

[11] Z.-H. Li and H.-X. Zhang. Study on gas kinetic unified algorithm for flows from rarefied transition to continuum. J. Comput. Phys., 193(2):708–738, 2004.

[12] S.S. Lo and S.K. Loyalka. An efficient computation of near-continuum rarefied gas flows. J. Applied Mathematics and Physics (ZAMP), 33:419–424, 1982.

[13] I.S. Men'shov and Y. Nakamura. An implicit advection upwind splitting scheme for hypersonic air flows in thermochemical nonequilibrium. In A Collection of Technical Papers of 6th Int. Symp. on CFD, volume 2, page 815. Lake Tahoe, Nevada, 1995.
[14] I.S. Men'shov and Y. Nakamura. On implicit Godunovs method with exactly linearized numerical flux. Computers and Fluids, 29(6):595–616, 2000.
[15] P.J. Roache. Verification and validation in computational science and engineering. 1998.
[16] V.A. Rykov. A model kinetic equation for a gas with rotational degrees of freedom. Fluid Dynamics, 10(6):959–966, 1975.
[17] E.M. Shakhov. Approximate kinetic equations in rarefied gas theory. Fluid Dynamics, 3(1):156–161, 1968.
[18] E.M. Shakhov. Generalization of the Krook kinetic relaxation equation. Fluid Dynamics, 3(5):142–145, 1968.
[19] F. Sharipov and V. Seleznev. Data on internal rarefied gas flows. J. Phys. Chem. Ref. Data, 27(3):657–706, 1998.
[20] F. Sharipov and V. Seleznev. Flows of rarefied gases in channels and microchannels. Russian Academy of Science, Ural Branch, Institute of Thermal Physics, 2008. in Russian.
[21] F.G. Sharipov. Rarefied gas flow through a long tube at any temperature ratio. J. Vac. Sci. Technol. A., 14(4):2627–2635, 1996.
[22] N.I. Tillaeva. A generalization of the modified Godunov scheme to arbitrary unstructured meshes. Transactions of the Central Aerohydrodynamics Institute, 17(2):18–26, 1986. in Russian.
[23] V.A. Titarev. Conservative numerical methods for model kinetic equations. Computers and Fluids, 36(9):1446 – 1459, 2007.
[24] V.A. Titarev. Numerical method for computing two-dimensional unsteady rarefied gas flows in arbitrarily shaped domains. Computational Mathematics and Mathematical Physics, 49(7):1197–1211, 2009.
[25] V.A. Titarev and E.M. Shakhov. Conservative TVD method for the calculation of the Poiseuille flow of rarefied gas in a channel of arbitrary cross section. Computational Mathematics and Mathematical Physics, 50(3), 2010, in press.
[26] V.A. Titarev and E.M. Shakhov. Numerical calculation of the hypersonic rarefied transverse flow past a cold flat plate. Fluid Dynamics, 40(5):790–804, 2005.
[27] J.J.W. van der Vegt and H. van der Ven. Discontinuous Galerkin finite element method with anisotropic local grid refinement for inviscid compressible flows. J. Comput. Phys., 141(1):46–77, 1998.
[28] J.Y. Yang and J.C. Huang. Rarefied flow computations using nonlinear model Boltzmann equations. J. Comput. Phys., 120(2):323–339, 1995.